The Plant Cell, Vol. 17, 849–858, March 2005, www.plantcell.org

Structural Basis for the Interaction between Pectin Methylesterase and a Specific Inhibitor Protein

Adele Di Matteo,[a,b] Alfonso Giovane,[c] Alessandro Raiola,[b,1] Laura Camardella,[d] Daniele Bonivento,[a] Giulia De Lorenzo,[b] Felice Cervone,[b] Daniela Bellincampi,[b,2] and Demetrius Tsernoglou[a]

[a] Department of Biochemical Sciences, University of Rome, 00185 Rome, Italy
[b] Department of Plant Biology, University of Rome, 00185 Rome, Italy
[c] Department of Biochemistry and Biophysics, Second University of Naples, I-80138, Naples, Italy
[d] Institute of Protein Biochemistry, Consiglio Nazionale delle Ricerche, I-80125, Naples, Italy

Pectin, one of the main components of the plant cell wall, is secreted in a highly methyl-esterified form and subsequently deesterified in muro by pectin methylesterases (PMEs). In many developmental processes, PMEs are regulated by either differential expression or posttranslational control by protein inhibitors (PMEIs). PMEIs are typically active against plant PMEs and ineffective against microbial enzymes. Here, we describe the three-dimensional structure of the complex between the most abundant PME isoform from tomato fruit (*Lycopersicon esculentum*) and PMEI from kiwi (*Actinidia deliciosa*) at 1.9-Å resolution. The enzyme folds into a right-handed parallel β-helical structure typical of pectic enzymes. The inhibitor is almost all helical, with four long α-helices aligned in an antiparallel manner in a classical up-and-down four-helical bundle. The two proteins form a stoichiometric 1:1 complex in which the inhibitor covers the shallow cleft of the enzyme where the putative active site is located. The four-helix bundle of the inhibitor packs roughly perpendicular to the main axis of the parallel β-helix of PME, and three helices of the bundle interact with the enzyme. The interaction interface displays a polar character, typical of nonobligate complexes formed by soluble proteins. The structure of the complex gives an insight into the specificity of the inhibitor toward plant PMEs and the mechanism of regulation of these enzymes.

INTRODUCTION

Pectin, one of the main components of the plant cell wall, is continually modified and remodeled during plant growth and development (Ridley et al., 2001). For example, the pattern of pectin esterification changes during cell expansion, growth, and fruit ripening as well as during infection by phytopathogenic microorganisms (Steele et al., 1997; Willats et al., 2001). After secretion into the wall as a highly methylesterified form, pectin is deesterified in muro by pectin methylesterases (PMEs) (E.C. 3.1.1.11) in a spatially regulated manner during development (Knox et al., 1990). Demethylation leads to the formation of polyuronides aggregating into calcium-linked gels that are important in controlling the porosity and mechanical properties of the wall (Willats et al., 2001). By generating free carboxylic groups, PMEs also affect the wall pH and consequently influence the activity of a wide range of hydrolytic enzymes, including PMEs (Grignon and Sentenac, 1991; Denes et al., 2000; Goldberg et al., 2001). PMEs produced by plants take part in important physiological processes, such as microsporogenesis, pollen growth, seed germination, root development, polarity of leaf growth, stem elongation, fruit ripening, and loss of tissue integrity (Tieman and Handa, 1994; Wen et al., 1999; Micheli et al., 2000; Pilling et al., 2000; Micheli, 2001; Pilling et al., 2004). They have also been reported to play a role in response to fungal pathogens (Wietholter et al., 2003) and are required for the systemic spread of *Tobacco mosaic virus* through the plant (Dorokhov et al., 1999; Chen et al., 2000; Chen and Citovsky, 2003). PMEs are not only produced by plants but also by microbial pathogens (De Lorenzo et al., 1997) and by symbiotic microorganisms during their interactions with plants (Lievens et al., 2002).

Isoforms of PME differing by molecular weight, pI, and biochemical activity are encoded by large families of genes, either constitutively expressed (Giovane et al., 1994; Gaffe et al., 1997; Micheli, 2001) or differentially regulated in specific tissues and developmental stages (Micheli et al., 2000; Micheli, 2001). In addition to the transcriptional control, a mechanism of regulation of PME activity is played by specific proteinaceous inhibitors, which were discovered in kiwi (*Actinidia deliciosa*) (Balestrieri et al., 1990; Giovane et al., 1995) and recently found also in *Arabidopsis thaliana* (Wolf et al., 2003; Raiola et al., 2004). These inhibitors, named PMEIs, typically inhibit PMEs of plant origin and do not affect the activity of microbial enzymes (Giovane et al., 2004).

Although a role of PMEIs in regulating the activity of endogenous PMEs is most likely, a physiological action of these inhibitors toward enzymes derived from different species cannot be excluded. It is known that PMEs and PMEIs are both expressed in flower tissues and pollen grains (Wolf et al., 2003; Markovic and Janecek, 2004; Raiola et al., 2004; L. Camardella, A. Giovane, and D. Bellincampi, unpublished results) and that wind and animal visitations continually bring pollen onto flowers

[1] Current address: Dipartimento del Territorio e Sistemi Agro-Forestali, Università di Padova, Italy.
[2] To whom correspondence should be addressed. E-mail daniela.bellincampi@uniroma1.it; fax 39-06-49912446.
The author responsible for distribution of materials integral to the findings presented in this article in accordance with the policy described in the Instructions for Authors (www.plantcell.org) is: Daniela Bellincampi (daniela.bellincampi@uniroma1.it).
Article, publication date, and citation information can be found at www.plantcell.org/cgi/doi/10.1105/tpc.104.028886.

of heterologous species. The kiwi inhibitor (AcPMEI, SwissProt accession number P83326) is very efficient against PME of tomato fruit (*Lycopersicon esculentum*) (PME-1, SwissProt accession number P14280) and forms a noncovalent 1:1 complex (Mattei et al., 2002).

To date, the structures of only two PMEs, one from carrot (*Daucus carota*) (PDB code 1GQ8) (Johansson et al., 2002) and one from the bacterium *Erwinia chrysanthemi* (PDB code 1QJV) (Jenkins et al., 2001), have been solved. Very recently, the structure of the PMEI from Arabidopsis (At-PMEI1) has been determined (Hothorn et al., 2004b), whereas structural information on the PME/PMEI complex is still lacking. Here, we report the crystal structure of the complex between a plant PME and its specific inhibitor PMEI at 1.9-Å resolution. This structure allows a detailed analysis of the mode of interaction between the two proteins in terms of specificity and sheds light into the regulation of pectin deesterification in plants.

RESULTS AND DISCUSSION

PMEI from kiwifruit is composed of different isoforms that are not easily separated by biochemical methods (Camardella et al., 2000; Mattei et al., 2002). To obtain an amount of homogeneous PMEI suitable for structural characterization, a synthetic gene was generated on the basis of the amino acid sequence of the prevalent PMEI isoform from kiwifruit (Camardella et al., 2000) and expressed in *Pichia pastoris*. The protein, purified to homogeneity, displayed chemical, physical, and spectral properties identical to those of the prevalent natural isoform from kiwi (Scognamiglio et al., 2003). The enzyme was mixed with a molar excess of inhibitor, and the resulting PME/PMEI complex was purified by ion exchange chromatography.

The three-dimensional structure of the complex was determined at 1.9-Å resolution using a combination of single isomorphous replacement and molecular replacement methods. Details about data collection, phasing, and refinement statistics are summarized in Table 1. The model, comprising 317 residues for PME, 151 for PMEI, and 462 water molecules, has been refined to an R factor of 20.0% and an R_{free} of 23.1% and has a good stereochemistry, with 99.8% of the residues lying either in the most favored or in the additional allowed regions of the Ramachandran plot (Table 1).

The Structure of Tomato PME Exhibits the Typical Fold of Pectic Enzymes

PME-1 from tomato belongs to family CE8 of the sequence-based classification of carbohydrate esterases (http://afmb.cnrs-mrs.fr/

Table 1. Data Collection, Phasing, and Refinement Statistics

Data Collection	Form A	Form B	K_2OsO_4
Space group	P41212	P3221	P41212
Unit cell dimensions	a = b = 120.26 Å; c = 97.29 Å; α = β = γ = 90°	a = b = 90.38 Å; c = 149.1 Å; α = β = 90.0°; γ = 120.0°	a = b = 120.53 Å; c = 97.40 Å; α = β = γ = 90°
Wavelength (Å)	1.2	0.99	1.2
Resolution limits (Å)	30.0 to 2.8	50.0 to 1.9	25.0 to 3.2
Reflections			
Total (*n*)	500,955	412,612	234,634
Unique (*n*)	18,126	56,180	12,321
Completeness (last shell)	100 (100)	97.5 (92.5)	99.7 (100)
Average I/σ (last shell)	17.9	19.4	16.0
R_{merge} (%)	0.062 (0.45)	0.082 (0.338)	0.076 (0.327)
Derivative			
Concentration (mM)			1.00
Soaking time (h)			6.00
FOM (before DM)[a]			0.45
FOM (after DM)			0.65
Refinement statistics		Ramachandran statistics	
Resolution (Å)	25.0 to 1.9	Percentage of residues in allowed regions	91.9
R_{work}	0.20	Percentage of residues in additional allowed	7.9
R_{free}	0.23	Percentage of residues in generously allowed	0.2
		Percentage of residues in not allowed	0.0
	Model		
	PME 317	Amino acid residues	
	PMEI 151	Amino acid residues	
	462	Water molecules	

[a] DM, density modification; FOM, figure of merit.

CAZY). The enzyme folds into a right-handed parallel β-helix, first observed in pectate lyase C (Yoder et al., 1993) and typical of pectic enzymes (Jenkins and Pickersgill, 2001) (Figure 1). The β-helix consists of seven complete coils, which have different lengths because the number of amino acids located in the loops connecting the β-strands is variable. Each coil consists of three β-strands that line up to form three extended parallel β-sheets called PB1, PB2, and PB3. T1 identifies the stack of turns between PB1 and PB2, T2 the stack between PB2 and PB3, and T3 those between PB3 and PB1. Letters following T identify the position of each turn with respect to the coil of the β-helix, whereas A corresponds to the first turn in the N-terminal region. Turns T1 (except for TB1) are short and mainly composed of residues in α_L-conformation and are responsible for the sharp bend between the sheets as observed in other parallel β-helix structures (Federici et al., 2001; Jenkins and Pickersgill, 2001). Turns T2 and T3 are generally longer and more variable; in particular, TF3 and most of T2 turns protrude from the central parallel β-helix to form the shallow cleft where the putative active site is located. In contrast with what was reported (Markovic and Jornvall, 1992), no electron density corresponding to the disulphide bridges Cys98-Cys125 and Cys166-Cys200 was observed. The absence of these bridges was confirmed by biochemical analysis, indicating the presence of four thiol groups upon titration with the Ellman's reagent in denaturing conditions (data not shown). The N-terminal region of PME is composed by a short α-helix followed by a β-strand that lines up with PB1. The C-terminal region has an extended conformation in which a long tail and four short and distorted α-helices protrude out of the parallel β-helix flanking PB1.

The putative active site of PME is located on the PB3 sheet in a cleft shaped by TB2, TC2, TF2, and TF3. Many aromatic residues (Phe80, Tyr135, Phe156, Tyr218, Trp223, and Trp248) putatively involved in substrate binding are located in this pocket (Johansson et al., 2002). These residues are well conserved in plant PMEs (Markovic and Janecek, 2004). Tyr135, Phe156, and Trp223 are also conserved in PME of *E. chrysanthemi* (Jenkins et al., 2001). Asp132, Asp153, and Arg 221, located inside the crevice, have been hypothesized to be the catalytic residues (Jenkins et al., 2001). In the putative catalytic site, OD1 of Asp153 is located 2.82 Å from and interacts with the NE of Arg221, whereas OD2 of Asp153 is located 2.85 Å from and interacts with NH2 of Arg221. Moreover, OD2 of Asp153 is at H-bonding distance (2.63 Å) from a water residue (W227) that also forms an H-bond with OD1 of Asp132 (2.76 Å) (Figure 2). In analogy with the proposed mechanism of action of PME from carrot (Johansson et al., 2002), we can infer a mechanism of catalysis in which Asp153, polarized by the proximity with Arg221, performs a nucleophilic attack on the carboxymethyl group of the substrate. The tetrahedral anionic intermediate formed is stabilized by the interaction with two conserved Gln residues (Gln109 and Gln131). Afterwards, Asp132 likely acts as a proton donor in the cleavage step where methanol is released. The resulting carboxylate group of Asp132 then behaves as a base and receives a proton from an incoming water molecule (W227), thus restoring the active site of the enzyme. An alternative hypothesis proposed by Johansson (Johansson et al., 2002) foresees a primary nucleophilic attack performed by the water molecule deprotonated both by Asp132 and Asp153.

Superimposition of the known PME structures of carrot, *E. chrysanthemi*, and tomato reveals the similarity of the overall folding topologies. The similarity of tomato and carrot PMEs is more extensive with a root mean square deviation (RMSD) value of 0.7 Å calculated for all Cα atoms (Figure 3A), whereas the bacterial enzyme can be well superimposed to tomato PME only for 284 Cα atoms out of 317 and with a higher RMSD value of 1.8 Å (Figure 3B). The main differences between the plant and the bacterial enzymes are located on TB2, TC2, TF2, TG3, and TH3; these turns protrude out of the β-helix and are much longer in the bacterial enzyme, making its putative active site cleft deeper and narrower than that of plant PMEs.

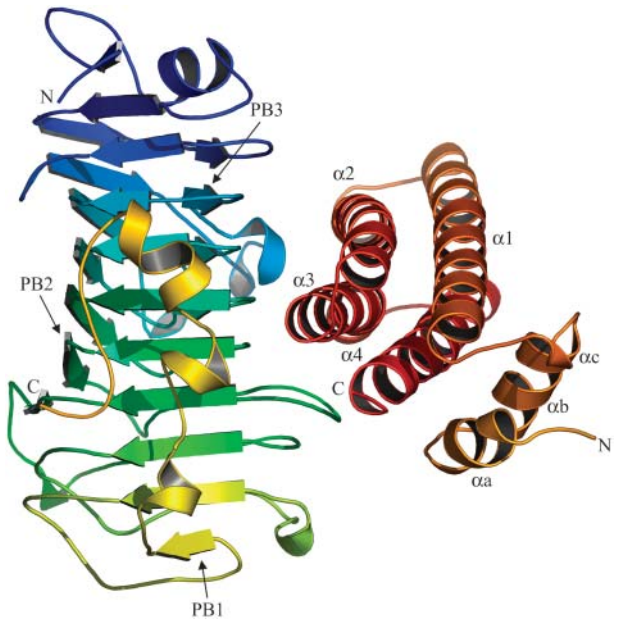

Figure 1. Structure of the PME-PMEI complex.

Ribbon representation illustrating the relative positions of PMEI and PME in the complex. The enzyme is shown in green–blue on the left side. The inhibitor is represented in yellow–red on the right side; the α-helices of the four-helix bundle are indicated as α1 to α4, whereas helices of the N-terminal region are named αa, αb, and αc. The inhibitor binds the active site region of the enzyme, hampering its access to the substrate.

The Inhibitor Folds in an Up-and-Down Four-Helical Bundle

PMEI is almost all helical, with four long helices (α1, α2, α3, and α4) aligned in an antiparallel manner in a classical up-and-down four-helical bundle (Figure 1). The interior of the bundle is stabilized by hydrophobic interactions and by a disulphide bridge between Cys74 and Cys114, which connects helices α2 and α3. The N-terminal region, composed of three short and distorted helices (αa, αb, and αc), extends outside the central domain and lines roughly parallel to the plane defined by the helices α1 and α4. A disulphide bridge between Cys9 and Cys18 connects αa and αb.

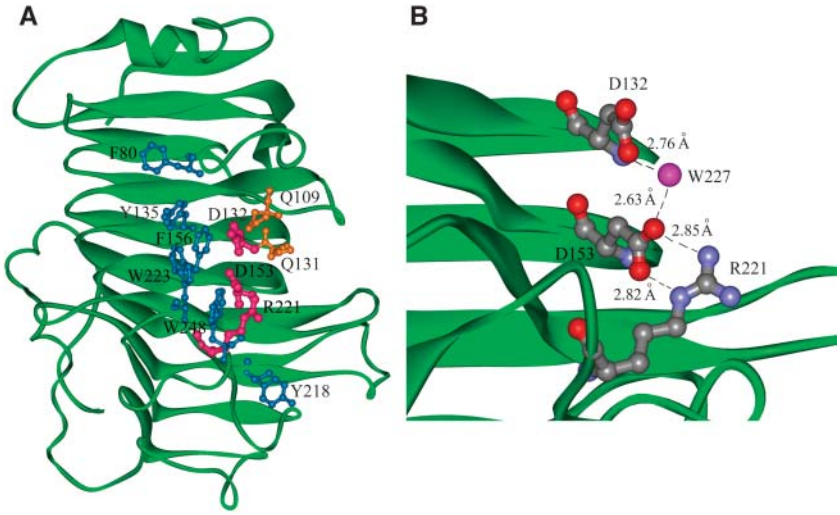

Figure 2. Close-Up View of the Tomato PME Active Site.

(A) Structure of tomato PME in which residues involved in catalysis (violet), in stabilization of the catalytic intermediate (orange), and in substrate binding (blue) are shown in ball and stick representation.
(B) Further close-up view representation of amino acid residues and a water molecule (blue ball) putatively involved in catalysis; H-bond pattern is highlighted.

According to sequence-based classification, PMEIs belong to the family PF04043 (Pfam database, http://pfam.wustl.edu/) of invertase inhibitor (INH)/PMEIs and share with INH several structural properties (Scognamiglio et al., 2003). Recently, the structure of an invertase inhibitor from tobacco (*Nicotiana tabacum*) (Nt-CIF) has been elucidated (PDB code 1RJ1) (Hothorn et al., 2004a) as well as the structure of a PMEI from Arabidopsis (At-PMEI1) (Hothorn et al., 2004b). Structural superimposition of PMEI from kiwi and Nt-CIF reveals a striking similarity between the two proteins, although their sequence identity is rather low (29.2%) (Figure 4). An RMSD value of 1.7 Å calculated on 144 Cα out of 151 confirms that the overall fold is very similar in both inhibitors. Main differences are located in the N-terminal region and in the loops connecting the helices of the bundle; notably an amino acid insertion, located in helix α2 of Nt-CIF partially distorts the helix (Figure 4). Structural superimposition between At-PMEI1 and AcPMEI is not possible because coordinates of At-PMEI1 are not yet available. However, considering the superimposition of At-PMEI1 and Nt-CIF (Hothorn et al., 2004b), the two inhibitors are quite similar in the bundle, whereas significant differences are located in the N-terminal extension. It is puzzling that the N-terminal region of AcPMEI folds back and packs with the bundle through hydrophobic interaction (Figure 1), whereas the N-terminal extension of At-PMEI1, which crystallizes in a dimeric form, packs against the bundle of another molecule (Hothorn et al., 2004b). Interestingly Pro-28 of At-PMEI1, which is located in the linker between the N-terminal region and the four-helix bundle and is responsible for the orientation of the N-terminal region, is replaced by a Lys in AcPMEI, suggesting that the different topology of the two inhibitors is due to the presence of different residues at the same position.

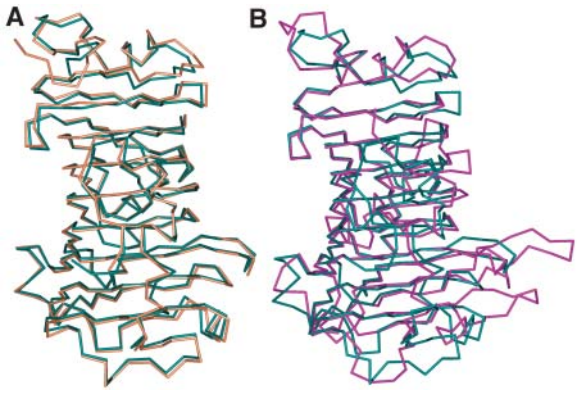

Figure 3. Comparison of the Known Structures of PMEs.

(A) Overlay of the Cα trace of PME from tomato (green) and PME from carrot (orange). Structures are almost completely superimposable, with a RMSD value of 0.7 Å, calculated on all Cα.
(B) Superimposition of PME from tomato (green) and PME from *E. chrysanthemi* (violet). The RMSD value, calculated on 284 out of 317 Cα, is 1.8 Å. Although the β-helices are completely superimposable, main differences are located in the length of the turns protruding out from the β-helix in proximity of the putative active site cleft.

The PME-PMEI Complex

PME and PMEI form a stoichiometric 1:1 complex in which the inhibitor covers the shallow cleft of the enzyme where the putative active site is located. The four-helix bundle of PMEI packs roughly perpendicular to the parallel β-helix of PME, and the three helices α2, α3, and α4, but not α1, interact with the enzyme in proximity of the putative active site (Figures 1 and 5)

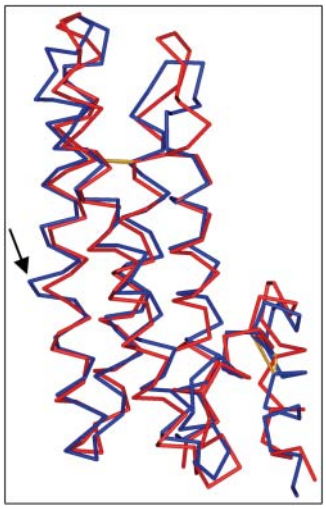

Figure 4. Structural Superimposition between PMEI and Nt-CIF.

PMEI (red) and Nt-CIF (blue) are superimposable, with a RMSD of 1.7 Å, calculated on 144 out of 151 Cα. Main differences are located in the loops connecting the helices of the bundle and in the N-terminal region; a distortion in the α2 helix of Nt-CIF is indicated by the arrow. Conserved disulphide bridges are represented in yellow.

The relative position of α2 and α3 helices is maintained by a disulphide bridge between Cys74 and Cys114. The N-terminal region of PMEI is poorly involved in the formation of the complex and may play a role in the structural stability of the inhibitor, as proposed for Nt-CIF (Hothorn et al., 2004a). Superimposition of the free Nt-CIF with the complexed PMEI shows a similar fold and orientation of helices in the bundle (Figure 4). Similarly, the structure of the free carrot PME is almost completely superimposable to the structure of tomato PME engaged in the complex with PMEI (Figure 3A). These features suggest that PME and PMEI do not undergo dramatic conformational changes upon formation of the complex.

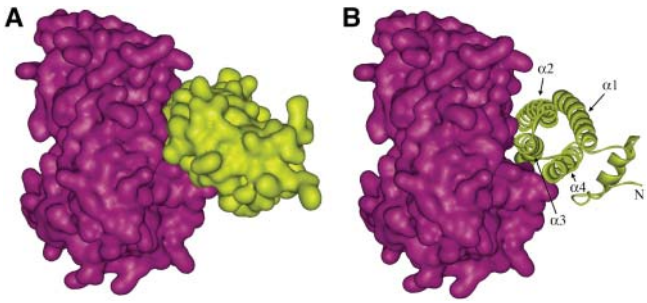

Figure 5. Molecular Surface of the PME-PMEI Complex.

(A) Representation of the molecular surface of the enzyme (violet) and the inhibitor (yellow) in the complex.
(B) Same view of the complex as in **(A)**, showing the molecular surface of PME and a ribbon diagram of PMEI. The α-helices α2, α3, and α4 of the inhibitor fit into the substrate binding cleft of the enzyme.

Upon interaction, PME and PMEI bury 1148 Å^2 and 1060 Å^2, respectively, of their accessible surface area (ASA). The total of 2208 Å^2 buried surface is somewhat larger than the average interface area reported for noncovalent protein complexes (ΔASA 1600 ± 400 Å^2) (LoConte et al., 1999). The interaction interface displays a surprisingly high polar character. No extended zones of hydrophobic interactions are present, whereas more than half (55%) of buried surface arises from polar and charged atoms (Figure 6). A large number of water molecules is present at the interface and 17 of them mediate intermolecular H-bonds (Figure 6). Such a polar character of the interface is typical of nonobligate complexes formed by soluble proteins, which need to expose a hydrophilic surface in their uncomplexed form (Jones and Thornton, 1996). Fifty residues (23 on PME and 27 on PMEI) establish contacts (Table 2). Twenty-two of these residues are engaged in H-bonds, and four form salt bridges (Table 3). Residues of PME forming contacts are mostly located in the proximity of the putative pectin binding site, particularly on PB3 and on T3 (Figure 2A). A large cluster of interacting residues is present on turns TD3 and TF3 and on the fourth strand of PB3. TB2 also participates with three residues contacting the inhibitor, whereas only one contact is present in the C-terminal tail of the enzyme. The contact residues of PMEI are mainly located on helices α2 and α3, with a continuous surface that extends all along. Ten residues are located on α2, 11 on α3, and four on α4; two residues reside on the N-terminal region of the inhibitor.

In the article by Hothorn et al. (2004b), the N-terminal region of At-PMEI1 has been proposed to be crucial for the interaction with PMEs. This model does not fit with our crystallographic structure of the PME-PMEI complex, and we cannot exclude that the mode of interaction of At-PMEI1 to PMEs is somewhat peculiar. Experimental data using chimeras between the N-terminal region of At-PMEI1 and the four-helix bundle of Nt-CIF indicate that ~100 times more quantity of the chimera is needed to obtain the same inhibition played by the natural At-PMEI1. This suggests that the four-helix bundle is also important for the interaction of At-PMEI1 and PME.

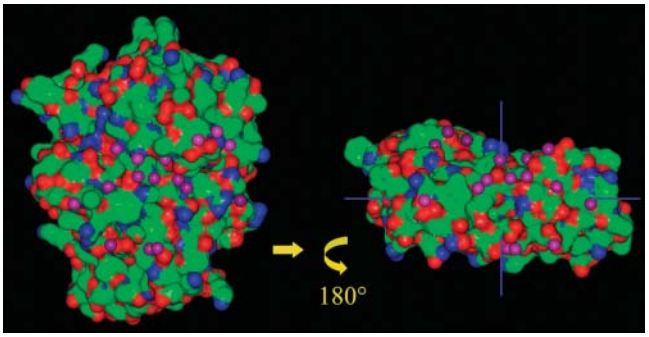

Figure 6. Representation of the Interacting Surface of PME and PMEI.

To open up the complex, PMEI has been shifted along its major axis and rotated by 180° around the vertical axis indicated. The molecular surfaces contributed by carbon atoms are in green, and those contributed by oxygen and nitrogen are in red and blue, respectively. Water molecules involved in water-mediated hydrogen bonds are represented as violet spheres.

Table 2. PME-PMEI Intermolecular Contacts

Enzyme Residues	Inhibitor Residues	Number of Contacts
Ser50	Asp83	3
Thr78	Thr73 Arg70 Gly69	8
Phe80	Thr73 Glu76 Asn77 Thr113	17
Arg81	Gly69 Glu72 Thr73 Glu76	13
Val88	Asp80	1
Gln90	Glu87 Tyr103	3
Asp118	Ile102 Tyr103	9
Tyr135	Thr113	1
His137	Asn77 Thr113	7
Ser138	Ala106	2
Gln139	Ser84 Ile102 Tyr103 Ala106	14
Arg140	Ser99 Ile102 Tyr103	13
Asn158	Asp109	6
Ala160	Ile102	1
Thr187	Arg13 Phe108	4
Asp188	Phe108 Asp140 Leu143	11
Asn190	Lys11 Asn101 Asp140 Leu143 Val144 Asn147	20
Gln191	Asn101 Ser105 Phe108 Asp109 Leu143	18
Ala192	Asn101 Ile102 Ser105	8
Thr193	Ser105	1
Trp223	Asp116	3
Lys224	Asp116	5
Gln299	Asn98	8

The number of atom–atom contacts at a distance of below 4.1 Å have been identified using the program Contact (CCP4).

Whereas the electrostatic potential surface of PMEI shows an acidic patch formed by Glu76, Asp80, and Asp83 on α2 helix and Asp 96, Asp109, and Asp116 on α3 helix, a positive counterpart is not found on the potential surface of PME. However, Asp116 (OD1 and OD2) and Glu76 (OE1) of PMEI are involved in salt bridges with Lys224 (NZ) and Arg81 (NE) of PME, respectively. The large interface area and the high number of direct and water-mediated H-bonds may account for the high stability of the PME-PMEI complex at physiological pH ($K_d = 5$ nM, pH 5.5) (Mattei et al., 2002).

The stability of the complex is pH dependent, being higher in acidic conditions, typical of the apoplastic environment, and decreasing drastically by raising the pH from 6.5 to 7.5; no formation of the complex occurs at pH 8.5 (D'Avino et al., 2003). The contact between the NE2 of His137 in PME and OG1 of Thr113 in the inhibitor (2.92 Å) may be crucial for determining the strength of the interaction in this pH range. The contribution of a high number of ionizable groups, the pK value of which is affected by their chemical environment, could also be important. Interestingly, at pH 6.0, the condition at which structure of the complex has been solved, OD1 of Asp140 in PMEI is located 2.4 and 3.21 Å from OD2 and OD1, respectively, of Asp188 in PME (Table 3). It is likely that, because of their proximity, at least one of them is protonated and acts as a hydrogen bond donor. Asp188 is located on the TF3 loop, where a wide patch of interacting residues that forms a network of intermolecular H-bonds (Asp188, Asn190, Gln191, and Ala192) is located (Table 2). We hypothesize that at higher pH values the deprotonation of an aspartic residue generates an electrostatic repulsion that loosens the H-bond network and destabilizes the complex. Interestingly, both PMEIs from Arabidopsis exhibit a Gly residue instead of Asp140 and form a complex with a lower pH dependence with tomato PME (Raiola et al., 2004).

Detailed analysis of residues involved in forming the complex reveals that the putative catalytic residues (Asp132, Asp153, and Arg221) do not establish contacts with the inhibitor, neither do Gln109 and Gln131, which are thought to stabilize the anionic intermediate formed after the first nucleophilic attack. Instead, three aromatic residues (Phe80, Tyr135, and Trp223), likely responsible for substrate binding, interact with the inhibitor. Remarkably, Phe80 is one of the residues mostly involved in the interaction, burying an area of 81 Å^2 upon formation of the complex. This residue establishes 17 contacts with four different residues of the inhibitor (Thr73, Glu76, Asn77, and Thr113) and a water-mediated hydrogen bond. Trp223 of PME forms three contacts with its interacting counterpart, whereas Tyr135 forms only one contact; moreover, each of them forms a water-mediated hydrogen bond. Upon formation of the complex with the inhibitor, Trp223 buries almost half of its solvent-exposed surface, and this explains the decrease of fluorescence observed in PME upon addition of the inhibitor (D'Avino et al., 2003). We can infer the mode of action of the inhibitor: on one hand, the inhibitor covers the active site cleft preventing the access of the substrate, and on the other hand, it prevents the interactions of Phe80, Tyr135, and Trp223 with the substrate. These observations are consistent with the observed competitive mode of inhibition. Notably, a similar mode of inhibition has been proposed for PGIP, a protein inhibitor of fungal polygalacturonases (De Lorenzo et al., 2001; Di Matteo et al., 2003), suggesting that

Table 3. Hydrogen Bonding and Salt Link Interaction between PME and PMEI in the Complex

PME	PMEI	Distance (Å)
Ser50 OG	Asp83 OD2	2.97
Thr78 OG1	Thr73 OG1	2.73
Arg81 NE	Glu76 OE1	3.81*
Asp118 OD2	Tyr103 OH	2.63
His137 NE2	Thr113 OG1	2.92
Gln139 NE2	Ser84 OG	3.21
Arg140 NH1	Ser99 OG	3.11
Arg140 NH2	Ser99 OG	2.85
Asn158 ND2	Asp109 OD2	2.63
Asp188 OD1	Asp140 OD1	3.21
Asp188 OD2	Asp140 OD1	2.40
Asn190 OD1	Asp140 OD1	2.97
Asn190 O	Asn101 ND2	2.93
Asn190 O	Asn147 ND2	3.10
Gln191 NE2	Asp109 OD1	3.20
Gln191 NE2	Ser105 O	3.24
Ala 192 N	Asn101 OD1	2.82
Lys224 NZ	Asp116 OD2	3.07*
Lys224 NZ	Asp116 OD1	2.93*

(*), Salt link interaction.

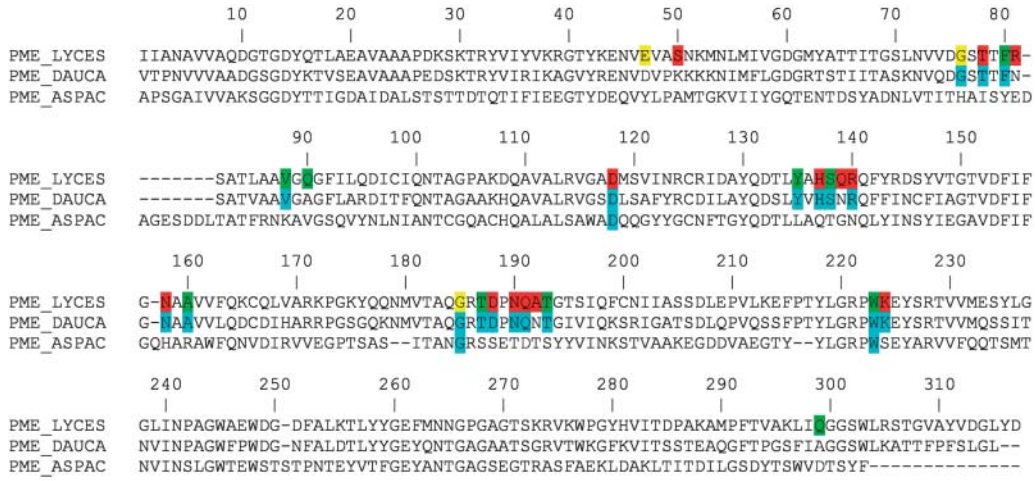

Figure 7. Sequence Comparison of PMEs from Tomato (PME_LYCES), Carrot (PME_DAUCA), and *A. aculeatus* (PME_ASPAC).

Residues involved in H-bonds (violet), Van der Waals contacts (green), and water-mediated H-bonds (yellow) with the inhibitor are shown. Conserved residues are in blue.

this may represent a general strategy evolved by plants for controlling pectic enzymes. Because mutations in residues involved in substrate binding affect enzyme activity, they are likely to be counter-selected during evolution. The involvement of these residues in the interaction with PMEI therefore minimizes the possibility for plant PMEs to escape recognition.

The structure of the PME-PMEI complex provides a possible explanation for the lack of inhibition of PMEIs on PMEs from the bacterium *E. crysanthemi* and the fungus *Aspergillus aculeatus* (Giovane et al., 2004; Raiola et al., 2004). In *E. crysanthemi*, the putative binding site cleft is much deeper than in plant-derived PMEs (Figure 3B). It is likely that the external loops of the bacterial enzyme create a steric hindrance that prevents the interaction with the inhibitor. On the other hand, the amino acid sequence alignment among PME from tomato, carrot, and *A. aculeatus* (Swiss-Prot code Q12535) reveals that almost all of the residues important for the interaction of tomato PME with the inhibitor are conserved in plant PMEs but not in the fungal enzyme, thus providing a reason for the observed lack of interaction (Figure 7).

PMEI and Nt-CIF exhibit an almost identical fold (Figure 4) but recognize different target enzymes. The structural view of the PME-PMEI complex also provides a possible explanation for the absence of interaction of Nt-CIF with PME. Sequence comparison between the PMEIs characterized so far and Nt-CIF shows that the subset of residues of the kiwi inhibitor, Asn101, Asp109, Thr113 (located on α3), and Asn147 (located on α4), which form intermolecular H-bonds with the enzyme, are conserved only in PMEIs. In addition, an amino acid insertion that produces a distortion of the α2 helix of Nt-CIF is close to residues corresponding to Asp82 and Ser83 in α2 of PMEI, which are involved in H-bonds with PME (Figures 4 and 8). We speculate that the lack of residues important for the formation of the complex as well as the distortion of α2 helix of Nt-CIF compared with that of PMEI are responsible for the lack of interaction between Nt-CIF and PME.

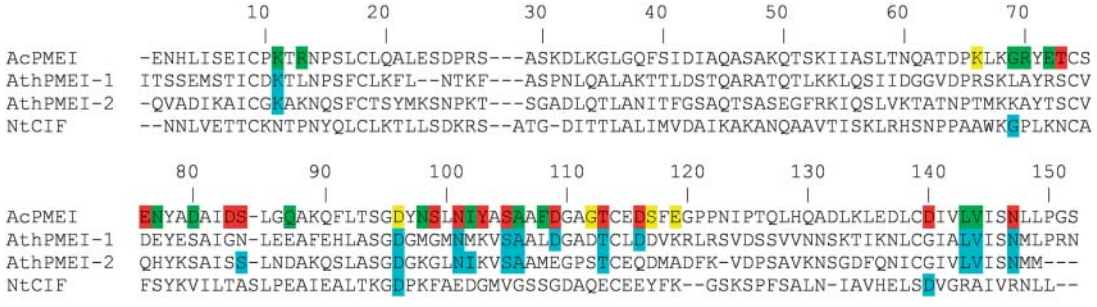

Figure 8. Sequence Comparison of PMEIs form Kiwi (AcPMEI), PMEIs from Arabidopsis (AthPMEI-1, Accession Number NP_175236; AthPMEI-2, Accession Number NP_188348), and Invertase Inhibitor from Tobacco (NtCIF).

Residues of the kiwi inhibitor involved in H-bonds (violet), Van der Waals contacts (green), and water-mediated H-bonds (yellow) with tomato PME are shown. Conserved residues are in blue.

METHODS

Expression and Purification of PMEI and PME

A synthetic *AcPMEI* gene was designed on the basis of the amino acid sequence of the mature PMEI from kiwifruit (*Actinidia deliciosa*) (AcPMEI accession number P83326 NCBI database) and expressed in *Pichia pastoris*. The synthesis of three *AcPMEI* DNA gene fragments was performed by PCR using PWO DNA Polymerase (Roche, Penzberg, Germany), and the entire gene was obtained by cloning the fragments into a pUC19 plasmid vector using two internal restriction sites designed to facilitate cloning. *AcPMEI* was amplified from pUC19 and cloned into the pPICZαA expression vector, used to transform *P. pastoris* strain X-33 (Invitrogen, Carlsbad, CA). The transformed cells were grown 3 d after induction with 0.5% (v/v) methanol; the supernatant of the culture was collected and total proteins precipitated with 80% (w/v) ammonium sulfate. The precipitated fraction was dissolved in 10 mM Tris-HCl, pH 7.5, dialyzed against the same buffer and loaded onto a Mono Q HR 10/10 column (Amersham Pharmacia Biosciences). AcPMEI was eluted by applying a linear gradient of 0 to 0.5 M NaCl in 10 mM Tris-HCl, pH 7.5. The eluted inhibitor was concentrated and loaded onto a HiLoad 16/60 Superdex 75 column (Amersham Pharmacia Biosciences) equilibrated in 10 mM Tris-HCl, pH 7.5, and 0.25 M NaCl. The purified inhibitor, displaying the same amino acid sequence of the prevalent natural isoform from kiwi, exhibited a single band by SDS-PAGE and showed a single peak upon reverse-phase HPLC on a Vydac C4 column. The N-terminal sequence of the protein confirmed its identity and indicated the presence of four additional amino acid residues, a remnant of the yeast signal sequence. These additional amino acids did not impair the inhibitory activity of the protein, and purified PMEI strongly inhibited PME-1 ($K_i = 28$ nM) (data not shown). The isoform PME-1 of tomato (*Lycopersicon esculentum*) (SwissProt accession number P14280) was purified as reported (Giovane et al., 1994). The inhibitory activity of AcPMEI against PME-1 was determined by automatic titration as previously described (Giovane et al., 1995). The inhibitory constant was calculated by Dixon plot using 0.3% and 0.05% citrus pectin (63 to 66% methylation degree from Sigma-Aldrich, St. Louis, MO).

Purification of the Complex

The PME-1/AcPMEI complex was obtained upon mixing PME-1 with a molar excess of AcPMEI in 20 mM sodium acetate, pH 5.5. The complex was purified by fast protein liquid chromatography on a Mono S HR 5/5 column (Amersham Pharmacia Biosciences) by applying a linear gradient of 0 to 0.5 M NaCl and concentrated through Centriplus YM-3 filters (Millipore, Bedford, MA).

Crystallization, X-Ray Data Collection, Structure Determination, and Refinement

The PME-PMEI complex crystallizes in two different crystal forms (A and B), both grown using the vapor-diffusion technique at 21°C. Form A was obtained when the solution of purified complex (11 mg/mL) was mixed 1:1 with a reservoir solution containing 2.5 M NaCl, 0.1 M sodium acetate, pH 4.5, and 0.2 M Li_2SO_4. Crystals appeared after 3 d and reached final dimensions of $\sim 0.4 \times 0.5 \times 0.5$ mm after 1 week. Crystals were transferred to a cryoprotectant solution consisting of 2.7 M NaCl, 0.1 M sodium acetate, pH 4.5, 0.2 M Li_2SO_4, and 22% polyethylene glycol 200 for 1 min, then looped from the drop and flash-frozen in a nitrogen stream at 100 K (Oxford Cryosystems, Oxford, UK). Diffraction data were collected to 2.8-Å resolution at the XRD Beamline of the ELETTRA Synchrotron (Trieste, Italy). Crystals of form A belong to the space group $P4_12_12$, with unit cell dimensions $a = b = 120.26$ Å, $c = 97.29$ Å, and $\alpha = \beta = \gamma = 90.0°$. Single crystals of form B were obtained in drops made up by 1 μL of 11.0 mg/mL of purified complex and 1 μL of well solution consisting of 1.6 M $MgSO_4$, and 0.1 M Mes, pH 6.0. After 1 week, crystals grew to $\sim 0.5 \times 0.6 \times 0.3$ mm. These crystals were flash-frozen in the presence of 25% (v/v) glycerol in mother liquor, and diffraction data were collected to 1.9-Å resolution at the XRD Beamline of the ELETTRA Synchrotron. Crystals of form B belong to the space group $P3_22_1$, with unit cell dimension of $a = b = 90.38$ Å, $c = 149.1$ Å, $\alpha = \beta = 90°$, and $\gamma = 120°$.

Initial phases were determined by single isomorphous replacement and anomalous scattering methods. The crystal of form A was soaked in a solution containing 2.5 M NaCl, 0.1 M sodium acetate, pH 4.5, 0.2 M Li_2SO_4, and 1 mM K_2OsO_4 for 6 h, cryoprotected as described above, and flash-frozen in liquid nitrogen. Data were collected at the BW7A Beamline of the Deutsches Elektronen Synchrotron (Hamburg, Germany). Oscillation images were integrated, scaled, and merged using DENZO and SCALEPACK (Otwinowski and Minor, 1996). The program SOLVE (Terwilliger, 1999) was used to perform heavy metal Patterson search with the derivatized and native crystal of form A, leading to an overall figure of merit of 0.45 at 30- to 3.5-Å resolution. Solvent flattening as implemented in the program RESOLVE (Terwilliger, 2000) was performed to improve the experimental map, yielding a figure of merit of 0.65 at 3.5-Å resolution. The resulting electron density map was sufficiently connected to build a partial model of the main chain of PMEI using QUANTA (Molecular Structure, Woodlands, TX). The structure of PME from carrot (*Daucus carota*) (PDB code 1GQ8) was used as a guide to locate the β-helix of the tomato PME into the density. No interpretable density for the N terminus and C terminus of PMEI as well as for all side chains of the inhibitor was available at this stage. The partially built model was then used as a template to perform a molecular replacement with native data of form B with the program AMORE (Navaza, 1994), obtaining a clear and interpretable electron density map at 1.9-Å resolution that was used to complete the tracing. The model was iteratively refined using REFMAC5 (Murshudov et al., 1997), subjected to a simulated annealing procedure as implemented in CNS (Adams et al., 1997), visually inspected, and manually rebuilt. Several water residues were added into the F_o-F_c density map, countered at 4σ, with the X-SOLVATE tool of QUANTA. Only solvent residues with a $B_{factor} \leq 45$ Å^2 and hydrogen bonded to the protein molecule were kept in the structure refinement. Further refinement and rebuilding led to a crystallographic R factor of 20% and an R_{free} of 23.1%. The final model contains residues 1 to 317 of chain A (PME), 0 to 150 of chain B (PMEI), and 462 water residues. A total of 91.9% of residues are in the most favored region of the Ramachandran space, with 7.9% in additional allowed regions, 0.2% in generously allowed regions, and none in disallowed regions. Secondary structure assignment and the check of the geometrical quality were performed using PROCHECK (Laskowski et al., 1993). The atomic coordinates have been deposited in the Protein Data Bank (www.pdb.org; PDB ID code 1XG2).

ACKNOWLEDGMENTS

We are grateful to Maurizio Brunori for is encouragement and valuable advice. We thank the staff at the ELETTRA Synchrotron (Trieste, Italy), the Deutsches Elektronen Synchrotron (Hamburg, Germany), and the European Synchrotron Radiation Facility (Grenoble, France) for beam time allocation and technical support. This research was supported by the European Union Gemini project (contract QLK1-2000-00911), the Institute Pasteur-Fondazione Cenci Bolognetti, the Giovanni Armenise-Harvard Foundation, and the Ministero dell'Università e della Ricerca Scientifica (PRIN 2002).

Received October 27, 2004; accepted December 28, 2004.

REFERENCES

Adams, P.D., Pannu, N.S., Read, R.J., and Brunger, A.T. (1997). Cross-validated maximum likelihood enhances crystallographic simulated annealing refinement. Proc. Natl. Acad. Sci. USA **94,** 5018–5023.

Balestrieri, C., Castaldo, D., Giovane, A., Quagliuolo, L., and Servillo, L. (1990). A glycoprotein inhibitor of pectin methylesterase in kiwi fruit (*Actinidia chinensis*). Eur. J. Biochem. **193,** 183–187.

Camardella, L., Carratore, V., Ciardiello, M.A., Servillo, L., Balestrieri, C., and Giovane, A. (2000). Kiwi protein inhibitor of pectin methylesterase amino-acid sequence and structural importance of two disulfide bridges. Eur. J. Biochem. **267,** 4561–4565.

Chen, M.-H., and Citovsky, V. (2003). Systemic movement of a tobamovirus requires host cell pectin methylesterase. Plant J. **35,** 386–392.

Chen, M.H., Sheng, J., Hind, G., Handa, A.K., and Citovsky, V. (2000). Interaction between the tobacco mosaic virus movement protein and host cell pectin methylesterases is required for viral cell-to-cell movement. EMBO J. **19,** 913–920.

D'Avino, R., Camardella, L., Christensen, T.M., Giovane, A., and Servillo, L. (2003). Tomato pectin methylesterase: Modeling, fluorescence, and inhibitor interaction studies-comparison with the bacterial (*Erwinia chrysanthemi*) enzyme. Proteins **53,** 830–839.

De Lorenzo, G., Castoria, R., Bellincampi, D., and Cervone, F. (1997). Fungal invasion enzymes and their inhibition. In The Mycota. V. Plant Relationships, Part B, G.C. Carroll and P. Tudzynski, eds (Berlin: Springer-Verlag), pp. 61–83.

De Lorenzo, G., D'Ovidio, R., and Cervone, F. (2001). The role of polygacturonase-inhibiting proteins (PGIPs) in defense against pathogenic fungi. Annu. Rev. Phytopathol. **39,** 313–335.

Denes, J.M., Baron, A., Renard, C.M., Pean, C., and Drilleau, J.F. (2000). Different action patterns for apple pectin methylesterase at pH 7.0 and 4.5. Carbohydr. Res. **327,** 385–393.

Di Matteo, A., Federici, L., Mattei, B., Salvi, G., Johnson, K.A., Savino, C., De Lorenzo, G., Tsernoglou, D., and Cervone, F. (2003). The crystal structure of PGIP (polygalacturonase-inhibiting protein), a leucine-rich repeat protein involved in plant defense. Proc. Natl. Acad. Sci. USA **100,** 10124–10128.

Dorokhov, Y.L., Makinen, K., Frolova, O.Y., Merits, A., Saarinen, J., Kalkkinen, N., Atabekov, J.G., and Saarma, M. (1999). A novel function for a ubiquitous plant enzyme pectin methylesterase: The host-cell receptor for the tobacco mosaic virus movement protein. FEBS Lett. **461,** 223–228.

Federici, L., Caprari, C., Mattei, B., Savino, C., Di Matteo, A., De Lorenzo, G., Cervone, F., and Tsernoglou, D. (2001). Structural requirements of endopolygalacturonase for the interaction with PGIP (polygalacturonase-inhibiting protein). Proc. Natl. Acad. Sci. USA **98,** 13425–13430.

Gaffe, J., Tiznado, M.E., and Handa, A.K. (1997). Characterization and functional expression of a ubiquitously expressed tomato pectin methylesterase. Plant Physiol. **114,** 1547–1556.

Giovane, A., Balestrieri, C., Quagliuolo, L., Castaldo, D., and Servillo, L. (1995). A glycoprotein inhibitor of pectin methylesterase in kiwi fruit. Purification by affinity chromatography and evidence of a ripening-related precursor. Eur. J. Biochem. **233,** 926–929.

Giovane, A., Quagliuolo, L., Servillo, L., Balestrieri, C., Laratta, B., and Castaldo, D. (1994). Purification and characterization of three isozymes of pectin methylesterase from tomato fruit. J. Food Biochem. **17,** 339–349.

Giovane, A., Servillo, L., Balestrieri, C., Raiola, A., D'Avino, R., Tamburrini, M., Ciardiello, M.A., and Camardella, L. (2004). Pectin methylesterase inhibitor. Biochim. Biophys. Acta **1696,** 245–252.

Goldberg, R., Pierron, M., Bordenave, M., Breton, C., Morvan, C., and Du Penhoat, C.H. (2001). Control of Mung bean pectinmethylesterase isoform activities. Influence of pH and carboxyl group distribution along the pectic chains. J. Biol. Chem. **276,** 8841–8847.

Grignon, C., and Sentenac, H. (1991). pH and ionic conditions in the apoplastic. Annu. Rev. Plant Physiol. Plant Mol. Biol. **42,** 103–128.

Hothorn, M., D'Angelo, I., Marquez, J.A., Greiner, S., and Scheffzek, K. (2004a). The invertase inhibitor Nt-CIF from tobacco: A highly thermostable four-helix bundle with an unusual N-terminal extension. J. Mol. Biol. **335,** 987–995.

Hothorn, M., Wolf, S., Aloy, P., Greiner, S., and Scheffzek, K. (2004b). Structural insights into the target specificity of plant invertase and pectin methylesterase inhibitory proteins. Plant Cell **16,** 3437–3447.

Jenkins, J., Mayans, O., Smith, D., Worboys, K., and Pickersgill, R.W. (2001). Three-dimensional structure of *Erwinia chrysanthemi* pectin methylesterase reveals a novel esterase active site. J. Mol. Biol. **305,** 951–960.

Jenkins, J., and Pickersgill, R. (2001). The architecture of parallel beta-helices and related folds. Prog. Biophys. Mol. Biol. **77,** 111–175.

Johansson, K., El Ahmad, M., Friemann, R., Jornvall, H., Markovic, O., and Eklund, H. (2002). Crystal structure of plant pectin methylesterase. FEBS Lett. **514,** 243–249.

Jones, S., and Thornton, J.M. (1996). Principles of protein-protein interactions. Proc. Natl. Acad. Sci. USA **93,** 13–20.

Knox, J.P., Linstead, P.J., King, J., Cooper, C., and Roberts, K. (1990). Pectin esterification is spatially regulated both within cell walls and between developing tissues of root apices. Planta **181,** 512–521.

Laskowski, R.A., MacArthur, M.W., Moss, D.S., and Thornton, J.M. (1993). PROCHECK—A program to check the stereochemical quality of protein structures. J. Appl. Crystallogr. **26,** 283–291.

Lievens, S., Goormachtig, S., Herman, S., and Holsters, M. (2002). Patterns of pectin methylesterase transcripts in developing stem nodules of *Sesbania rostrata*. Mol. Plant Microbe Interact. **15,** 164–168.

LoConte, L., Chothia, C., and Janin, J. (1999). The atomic structure of protein-protein recognition sites. J. Mol. Biol. **285,** 2177–2198.

Markovic, O., and Janecek, S. (2004). Pectin methylesterases: Sequence-structural features and phylogenetic relationships. Carbohydr. Res. **339,** 2281–2295.

Markovic, O., and Jornvall, H. (1992). Disulfide bridges in tomato pectinesterase: Variations from pectinesterases of other species; conservation of possible active site segments. Protein Sci. **1,** 1288–1292.

Mattei, B., Raiola, A., Caprari, C., Federici, L., Bellincampi, D., De Lorenzo, G., Cervone, F., Giovane, A., and Camardella, L. (2002). Studies on plant inhibitors of pectin modifying enzymes: Polygalacturonase-inhibiting protein (PGIP) and pectin methylesterase inhibitor (PMEI). In Carbohydrate Bioengineering: Interdisciplinary Approaches, T.T. Teeri, B. Svensson, H.J. Gilbert, and T. Feizi, eds (Cambridge, UK: Royal Society of Chemistry), pp. 160–167.

Micheli, F. (2001). Pectin methylesterases: Cell wall enzymes with important roles in plant physiology. Trends Plant Sci. **6,** 414–419.

Micheli, F., Sundberg, B., Goldberg, R., and Richard, L. (2000). Radial distribution pattern of pectin methylesterases across the cambial region of hybrid aspen at activity and dormancy. Plant Physiol. **124,** 191–199.

Murshudov, G.N., Vagin, A.A., and Dodson, E.J. (1997). Refinement of macromolecular structures by the maximum-likelihood method. Acta Crystallogr. D Biol. Crystallogr. **53,** 240–255.

Navaza, J. (1994). AMoRe: An automated package for molecular replacement. Acta Crystallogr. D Biol. Crystallogr. **50,** 157–163.

Otwinowski, Z., and Minor, W. (1996). Processing of x-ray: Diffraction data collected in oscillation mode. In Methods in Enzymology, C.W.

Carter and R.M. Sweet, eds (London and New York: Academic Press), pp. 307–326.

Pilling, J., Willmitzer, L., Bucking, H., and Fisahn, J. (2004). Inhibition of a ubiquitously expressed pectin methyl esterase in *Solanum tuberosum* L. affects plant growth, leaf growth polarity, and ion partitioning. Planta **219,** 32–40.

Pilling, J., Willmitzer, L., and Fisahn, J. (2000). Expression of a *Petunia inflata* pectin methyl esterase in *Solanum tuberosum* L. enhances stem elongation and modifies cation distribution. Planta **210,** 391–399.

Raiola, A., Camardella, L., Giovane, A., Mattei, B., De Lorenzo, G., Cervone, F., and Bellincampi, D. (2004). Two *Arabidopsis thaliana* genes encode functional pectin methylesterase inhibitors. FEBS Lett. **557,** 199–203.

Ridley, B.L., O'Neill, M.A., and Mohnen, D. (2001). Pectins: Structure, biosynthesis, and oligogalacturonide-related signaling. Phytochemistry **57,** 929–967.

Scognamiglio, M.A., Ciardiello, M.A., Tamburrini, M., Carratore, V., Rausch, T., and Camardella, L. (2003). The plant invertase inhibitor shares structural properties and disulfide bridges arrangement with the pectin methylesterase inhibitor. J. Protein Chem. **22,** 363–369.

Steele, N.M., McCann, M.C., and Roberts, K. (1997). Pectin modification in cell walls of ripening tomatoes occurs in distinct domains. Plant Physiol. **114,** 373–381.

Terwilliger, T.C. (1999). Reciprocal-space solvent flattening. Acta Crystallogr. D Biol. Crystallogr. **55,** 1863–1871.

Terwilliger, T.C. (2000). Maximum-likelihood density modification. Acta Crystallogr. D Biol. Crystallogr. **56,** 965–972.

Tieman, D.M., and Handa, A.K. (1994). Reduction in pectin methylesterase activity modifies tissue integrity and cation levels in ripening tomato (*Lycopersicon esculentum* Mill.) fruits. Plant Physiol. **106,** 429–436.

Wen, F.S., Zhu, Y.M., and Hawes, M.C. (1999). Effect of pectin methylesterase gene expression on pea root development. Plant Cell **11,** 1129–1140.

Wietholter, N., Graessner, B., Mierau, M., Mort, A.J., and Moerschbacher, B.M. (2003). Differences in the methyl ester distribution of homogalacturonans from near-isogenic wheat lines resistant and susceptible to the wheat stem rust fungus. Mol. Plant Microbe Interact. **16,** 945–952.

Willats, W.G., Orfila, C., Limberg, G., Buchholt, H.C., van Alebeek, G.J., Voragen, A.G., Marcus, S.E., Christensen, T.M., Mikkelsen, J.D., Murray, B.S., and Knox, J.P. (2001). Modulation of the degree and pattern of methyl esterification of pectic homogalacturonan in plant cell walls. Implications for pectin methyl esterase action, matrix properties and cell adhesion. J. Biol. Chem. **276,** 19404–19413.

Wolf, S., Grsic-Rausch, S., Rausch, T., and Greiner, S. (2003). Identification of pollen-expressed pectin methylesterase inhibitors in Arabidopsis. FEBS Lett. **555,** 551–555.

Yoder, M.D., Keen, N.T., and Jurnak, F. (1993). New domain motif: The structure of pectate lyase C, a secreted plant virulence factor. Science **260,** 1503–1507.